NACA

RESEARCH MEMORANDUM

LONGITUDINAL STABILITY CHARACTERISTICS AT TRANSONIC SPEEDS

OF A CANARD CONFIGURATION HAVING A 45° SWEPTBACK WING

OF ASPECT RATIO 6.0 AND NACA 65A009 AIRFOIL SECTION

By A. James Vitale and John C. McFall, Jr.

Langley Aeronautical Laboratory
Langley Field, Va.

NATIONAL ADVISORY COMMITTEE
FOR AERONAUTICS
WASHINGTON
November 15, 1954

~~CONFIDENTIAL~~

NATIONAL ADVISORY COMMITTEE FOR AERONAUTICS

RESEARCH MEMORANDUM

LONGITUDINAL STABILITY CHARACTERISTICS AT TRANSONIC SPEEDS

OF A CANARD CONFIGURATION HAVING A 45° SWEPTBACK WING

OF ASPECT RATIO 6.0 AND NACA 65A009 AIRFOIL SECTION

By A. James Vitale and John C. McFall, Jr.

SUMMARY

A flight investigation has been conducted to determine the longitudinal stability, lift, and drag characteristics at transonic speeds of a rocket-powered model of a canard configuration having a 45° sweptback wing of aspect ratio 6.0, taper ratio of 0.6, and NACA 65A009 airfoil section. The canard surface had an aspect ratio of 4.0 and 45° of sweepback. The variations with Mach number of lift, drag, and longitudinal stability for the canard configuration are compared with a tailless and a conventional or tail-last model having the same wing.

Large changes in aerodynamic-center position and damping in pitch in the transonic region were present for the tailless, tail-last, and canard configurations. The aerodynamic-center position showed the trend of a forward movement with increasing Mach number for the canard configuration.

INTRODUCTION

A study of the merits of a canard configuration over the conventional type of aircraft has been made in reference 1. Experimental studies of various canard configurations have continued because of possible advantages in stability and control at high speeds. This paper presents the longitudinal stability, lift, and drag characteristics at transonic speeds of a canard configuration having a 45° sweptback wing of aspect ratio 6.0 and a horizontal canard surface of aspect ratio 4.0 and 45° of sweepback. In addition, comparisons are made with experimental results for a conventional-type or tail-last configuration (ref. 2) and a tailless configuration (ref. 3), both having wing and tail surfaces of the same plan form, respectively. Since some differences such as structural flexibility, center-of-gravity position, and

~~CONFIDENTIAL~~

tail length existed between the various configurations, the comparisons made are more qualitative than quantitative, and emphasis is placed on comparing the variation with Mach number of static longitudinal stability, lift-curve slope, low-lift trim drag, and damping-in-pitch derivative for the canard, tail-last, and tailless configurations.

The experimental results for the canard configuration were obtained from the tests of a rocket-powered model at the Langley Pilotless Aircraft Research Station at Wallops Island, Va. The model was disturbed in pitch with small pulse rockets fired at time intervals during the flight. The data were obtained over a Mach number range of 0.80 to 1.30 and near zero lift coefficient.

In addition to experimental results the loss in lift due to aero-elastic wing deflection was calculated by the method of reference 4.

SYMBOLS

α angle of attack, deg

A aspect ratio

a.c.   aerodynamic center, percent $\bar{c}$, positive behind leading edge of $\bar{c}$

c chord, ft

$\bar{c}$ mean aerodynamic chord, ft

$C_{D_{trim}}$ drag coefficient near trim, $C_N \approx 0$

C_m pitching-moment coefficient

a_n normal acceleration as obtained from accelerometer, ft/sec^2

C_N normal force coefficient, $\dfrac{a_n}{g}\dfrac{W}{sq}$

g acceleration of gravity, 32.2 ft/sec^2

$C_{m_q} + C_{m_{\dot{\alpha}}}$ pitch-damping derivatives, per radian

K factor for converting flexible-wing lift data to rigid conditions

M	Mach number
q	free-stream dynamic pressure, lb/sq ft
P	period of oscillation, sec
R	Reynolds number based on wing $\bar{c}$
S	total wing area, sq ft
W	weight, lb
$T_{1/2}$	time for oscillation to damp to one-half amplitude, sec
V	velocity, ft/sec
θ	angle of pitch, radians

$$C_{m_q} = \frac{dC_m}{d\left(\frac{q\bar{c}}{2V}\right)}$$

$$C_{m_{\dot{\alpha}}} = \frac{dC_m}{d\left(\frac{\dot{\alpha}\bar{c}}{2V}\right)}$$

$$\dot{\alpha} = \frac{1}{57.3}\frac{d\alpha}{dt}$$

$$q = \frac{d\theta}{dt}$$

MODEL AND APPARATUS

Model

The model tested was a canard configuration having a wing with quarter-chord sweep of 45°, aspect ratio 6.0, taper ratio 0.6, and NACA 65A009 airfoil section. The canard surfaces had 45° of sweepback at the quarter-chord line, aspect ratio 4.0, taper ratio 0.4, and NACA 65A006 airfoil section. The fuselage fineness ratio was 12.7 and its ordinates are given in table I. The physical characteristics and the longitudinal distribution of area of the model are shown in figure 1 and photographs of the model are presented in figure 2. Two flat-plate fins were used to stabilize the model directionally.

The model wing was of composite construction having 0.064-inch-thick Inconel surface inlays and was identical in construction to the wing of model 1 in reference 3. The canard surfaces were constructed of a solid 24S-T aluminum-alloy core with a thin veneer of wood on the surface and were fixed on the model at zero incidence.

The mass characteristics of the model are given in the following table:

Weight, lb 83.4
Moment of inertia (pitch), slug-ft^2 . . . . 9.8
Center-of-gravity position, percent $\bar{c}$ (ahead of leading
    edge of $\bar{c}$). . . . . -129.2

INSTRUMENTATION

The model was equipped with a standard NACA 4-channel telemeter transmitting continuous measurements of normal acceleration, angle of attack, and total pressure.

A vane-type instrument mounted on a sting extending from the nose of the model (fig. 2) was used to measure angle of attack. The total-pressure pickup for measuring Mach number was mounted on a small strut below the fuselage (fig. 2(a)). Normal acceleration was measured at the model center of gravity and 2.86 feet ahead of the model center of gravity.

Ground apparatus included radiosonde, motion-picture cameras, CW Doppler radar unit, and a tracking radar unit.

TESTS AND ANALYSIS

Tests

Structural influence coefficients for the wing were measured to permit determination of aeroelastic properties. Model natural frequencies and modes of vibration were obtained by recording the response of the model to vibrations of known frequency applied by a mechanical shaker. The frequencies measured for the canard configuration were as follows:

Wing first bending, cps 35
Wing second bending, cps 144
Canard first bending, cps 97

The model was launched at approximately 60° from the horizontal using a rail-type launcher (fig. 3). A 65-inch HVAR rocket motor was used to boost the model to $M = 1.0$. At booster burnout the model separated from the booster and a 3.25-inch rocket sustainer motor accelerated the model to $M = 1.4$.

During the decelerating portion of flight the model experienced short-period oscillations in angle of attack following each pulse rocket disturbance.

Mach number and dynamic pressure were calculated from both telemetered total pressure with radiosonde static pressure and Doppler radar velocity. Reynolds number (based on wing $\bar{c}$ and dynamic pressure) obtained during the flight is shown as figure 4.

ANALYSIS

Time histories of the model short-period oscillations in angle of attack and normal acceleration were analyzed by the method of reference 5 to obtain longitudinal stability and lift characteristics. The instantaneous pitching moment was obtained by means of two normal accelerometers located at the center of gravity and in the nose of the model and the data were reduced by the method given in reference 4.

Since the model was not equipped with a longitudinal accelerometer the lift data are presented as normal-force coefficients, and for the low angles of attack of this test C_N is approximately equal to C_L. Model trim drag characteristics were obtained from Doppler radar velocity. From the drag polars of reference 2 it can be seen that $C_{D_{trim}}$ is nearly equal to the minimum drag coefficient for this test.

Using the method of reference 4 the effect of aeroelastic distortion on the lift-curve slope of the exposed wing was calculated for the canard and also for the tail-last and tailless configurations. The bending stiffnesses of the wings tested on the canard and tailless models were equal since the wings were constructed identically. The wings for both of these models were also nearly equal to the bending stiffness of the solid dural wing of the tail-last model. However, the loss in lift due to the wing deflecting in flight was not the same for all three models. Due to angular acceleration in pitch, the normal acceleration experienced by the wing is greater than the model center-of-gravity normal acceleration if the wing is located behind the model center of gravity. For this reason, the effect of wing-inertia loading acting in opposition to aerodynamic loading was different for the three

models. In addition, the span load of the canard model wing differed
from the other two models because the downwash from the canard surface
increased the load on the outboard portion of the wing for the canard
model.

An attempt was made to include these effects in calculating the
loss in lift of the exposed wing for the three models. This increment
in exposed-wing lift-curve slope was added to the measured total model
lift-curve slope to obtain the factor shown in figure 5 for converting
the lift-curve. slopes of the three models to the rigid-wing values.
The values shown for the tailless model are different from those pre-
sented in reference 3 because the pitching-inertia effect was not
accounted for in reference 3.

ACCURACY

The possible systematic errors in the absolute values of C_N as
affected by instrument calibration ranges are as follows:

M	C_N
1.2	±0.002
1.0	±.003
.8	±.005

The $C_{D_{trim}}$ values were obtained from Doppler radar velocity
measurements and are thought to be accurate to ±0.0010 at supersonic
speeds and ±0.0015 at subsonic speeds.

The Mach numbers are accurate to ±1 percent at supersonic speeds
and ±2 percent at subsonic speeds. Further errors in the aerodynamic
coefficients may arise from possible dynamic pressure inaccuracies which
are approximately twice as great as errors in Mach number.

Errors in measured angle of attack are independent of dynamic
pressure and are not likely to vary with Mach number. The absolute
values of angle of attack as affected by instrument calibration ranges
are estimated to be accurate to ±0.2°. An indication of random errors
may be noted from the scatter of data points in the plots of
coefficients.

RESULTS AND DISCUSSION

Lift

The basic lift data are shown in figure 6 for the canard config-
uration of this test. In figure 6 the model normal-force coefficients
are plotted against angle of attack for Mach numbers from 0.79 to 1.30.
As shown in figure 6 the lift curves are linear in the low lift range
of approximately ±0.10 normal-force coefficient covered in this test.

The variation of lift-curve slope with Mach number measured for
the canard configuration is shown in figure 7. Also shown in figure 7
are the lift-curve slopes of the canard, tail-last (ref. 2), and tail-
less (ref. 3) configurations corrected to the rigid-wing values by
means of the factors shown in figure 5. A comparison of the rigid
lift-curve slopes of the canard and tail-last configurations indicates
that from a Mach number of 0.95 to 1.3 the canard-configuration lift-
curve slope is about 10 percent lower than the tail-last configuration.
A further examination of figure 7 shows that the tailless configuration
has a high lift-curve slope below a Mach number of 1.10 when compared
with the results from the canard and tail-last configurations. A
possible reason for this is that the tailless model had a weak fuselage
section where the pulse rockets were mounted, resulting in fuselage
bending under inertia loads which would cause the angle-of-attack
measurements to be low and the measured lift-curve slopes to be high.
Also, at subsonic speeds the error in Mach number could be as great as
±2 percent for all models giving a ±4 percent error in dynamic pressure
and a corresponding error in lift-curve slope.

Trim Drag

The variation of the low-lift trim drag coefficients with Mach
number is presented in figure 8 for the canard, the tail-last, and the
tailless configurations. The comparison is considered good since the
tail-last had more vertical tail area and a larger fuselage than the
canard and both the tail-last and the canard had more surface area than
the tailless configuration. The canard and tailless configurations
have about the same transonic drag rise and somewhat less than the drag
rise of the tail-last configuration.

Static Stability

The values of period of the short-period oscillations measured
from the angle-of-attack time history are shown in figure 9(a) and
converted to the variation of C_{m_α} with Mach number in figure 9(b).

The data of figure 9(b) show a decrease in pitching-moment-curve slope from -0.080 at a Mach number of 1.04 to -0.025 at a Mach number of 1.30.

Shown in figure 10 is the variation of pitching-moment coefficient with normal-force coefficient for the canard configuration at Mach numbers from 0.79 to 1.30. The pitching-moment curves for Mach numbers 1.19 and 1.30 are nonlinear with normal-force coefficient, with the curve for $M = 1.19$ having an unstable slope at zero normal force. From Mach numbers 1.01 to 0.79 the pitching-moment curves are fairly linear over the range of ±0.10 normal-force coefficient.

Since the method of obtaining C_{m_α} from the period of oscillation depends on the pitching-moment curves being linear, the values of $\frac{dC_m}{dC_N}$ obtained by dividing the C_{m_α} values of figure 9(b) by the C_{N_α} values of figure 7 are also shown in figure 10 as passing through the trim normal-force coefficient where the period data were taken. Where the pitching moments are nonlinear with lift coefficient the slopes obtained from the period of the oscillations agree with the pitching-moment data in the region near trim normal-force coefficient.

The static stability characteristics of the canard, tailless, and tail-last configurations are compared in the plot of aerodynamic-center position against Mach number in figure 11. The stability data of figure 11 were obtained from the period of the oscillations for all three configurations. As previously mentioned this comparison is primarily qualitative since the models differed in wing aeroelasticity.

Following a rearward peak in aerodynamic-center position near $M = 1.0$ all three configurations show a rapid forward movement in aerodynamic center. This is apparently a characteristic of the 9-percent-thick 45° swept wing. In addition, figure 11 shows a rearward trend of aerodynamic center with increasing Mach number for the tail-last configuration as would be expected, while the trend with increasing Mach number for the canard configuration is a forward movement. This forward movement for the canard could be desirable from several considerations, for example, the maneuverability at supersonic speeds.

Dynamic Stability

The time for the short-period oscillation to damp to one-half amplitude plotted against Mach number is shown as figure 12(a). The nonlinear portion of the data above $M = 1.0$ is shown as a dashed faired curve.

Figure 12(b) shows the trends with Mach number of the pitch-damping derivatives, $C_{m_q} + C_{m_{\dot{\alpha}}}$, for the canard, the tailless, and the tail-last configurations. The comparison is made to show only the trends since the models were tested with different center-of-gravity positions and tail lengths. The three models exhibit an erratic variation of $C_{m_q} + C_{m_{\dot{\alpha}}}$ in the transonic region which appears to be associated with 45° swept wings (ref. 6).

Trim Characteristics

The variations of trim angle of attack and trim normal-force coefficient with Mach number are presented as figures 13(a) and 13(b). The trim changes from $M = 1.14$ to $M = 1.3$ are also indicated on the nonlinear pitching-moment curves of figure 10 for $M = 1.3$ and 1.19.

CONCLUSIONS

Results from an investigation of the low-lift longitudinal stability, lift, and drag characteristics of a canard configuration having a 9-percent-thick, high-aspect-ratio sweptback wing and comparisons with data from a tailless and tail-last configuration having wing and tail surfaces of the same plan form indicated the following conclusions:

1. Over the Mach number range of 0.80 to 1.30 there was some reduction in lift-curve slope caused by adding the tail in front of the wing as compared to a conventional or tail-last configuration.

2. There was no large effect on the low-lift trim drag coefficient caused by adding a canard surface.

3. The variation of aerodynamic-center position with Mach number for the canard showed the trend of a forward movement with increasing Mach number. From a consideration of better maneuverability at supersonic speeds this variation could be desirable.

4. Large changes in the damping-in-pitch derivatives $C_{m_q} + C_{m_{\dot{\alpha}}}$ in the transonic region were present for the canard, tail-last, and tailless configurations.

5. Nonlinear pitching-moment curves and associated trim changes were present at $M = 1.19$ and $M = 1.30$.

Langley Aeronautical Laboratory,
      National Advisory Committee for Aeronautics,
            Langley Field, Va., August 17, 1954.

REFERENCES

1. Mathews, Charles W.: Study of the Canard Configuration With Particular Reference to Transonic Flight Characteristics and Low-Speed Characteristics at High Lift. NACA RM L8G14, 1949.

2. McFall, John C., Jr.: Longitudinal Stability Characteristics at Transonic Speeds of a Rocket-Propelled Model of an Airplane Configuration Having a 45° Swept Wing of Aspect Ratio 6.0. NACA RM L53G22a, 1954.

3. Walters, Richard E.: Comparison of Experimental With Calculated Results for the Lifting Effectiveness of a Flexible 45° Sweptback Wing of Aspect Ratio 6.0 at Mach Numbers From 0.8 to 1.3. NACA RM L54B16, 1954.

4. Vitale, A. James: Effects of Wing Elasticity on the Aerodynamic Characteristics of an Airplane Configuration Having 45° Sweptback Wings As Obtained From Free-Flight Rocket-Model Tests at Transonic Speeds. NACA RM L52I30, 1953.

5. Gillis, Clarence L., Peck, Robert F., and Vitale, A. James: Preliminary Results From a Free-Flight Investigation at Transonic and Supersonic Speeds of the Longitudinal Stability and Control Characteristics of an Airplane Configuration With a Thin Straight Wing of Aspect Ratio 3. NACA RM L9K25a, 1950.

6. Gillis, Clarence L., and Chapman, Rowe, Jr.: Summary of Pitch-Damping Derivatives of Complete Airplane and Missile Configurations As Measured in Flight at Transonic and Supersonic Speeds. NACA RM L52K20, 1953.

TABLE I

FUSELAGE ORDINATES

Station, in.	Radius, in.
1.00	.342
2.00	.578
4.00	.964
6.00	1.290
8.00	1.577
12.00	2.094
16.00	2.472
20.00	2.773
22.00	2.892
22.75	2.933
24.00	2.993
28.00	3.146
32.00	3.250
36.00	3.314
40.00	3.334
↓	↓
57.30	3.334
61.30	3.304
65.30	3.219
69.30	3.074
73.30	2.873
77.30	2.658
81.30	2.450
84.00	2.305
85.00	2.250

.25 chord line

45°

45°

57.89

22.80   6.67

$\bar{c}$

26.11

54.93

56.84

67.65

85.00
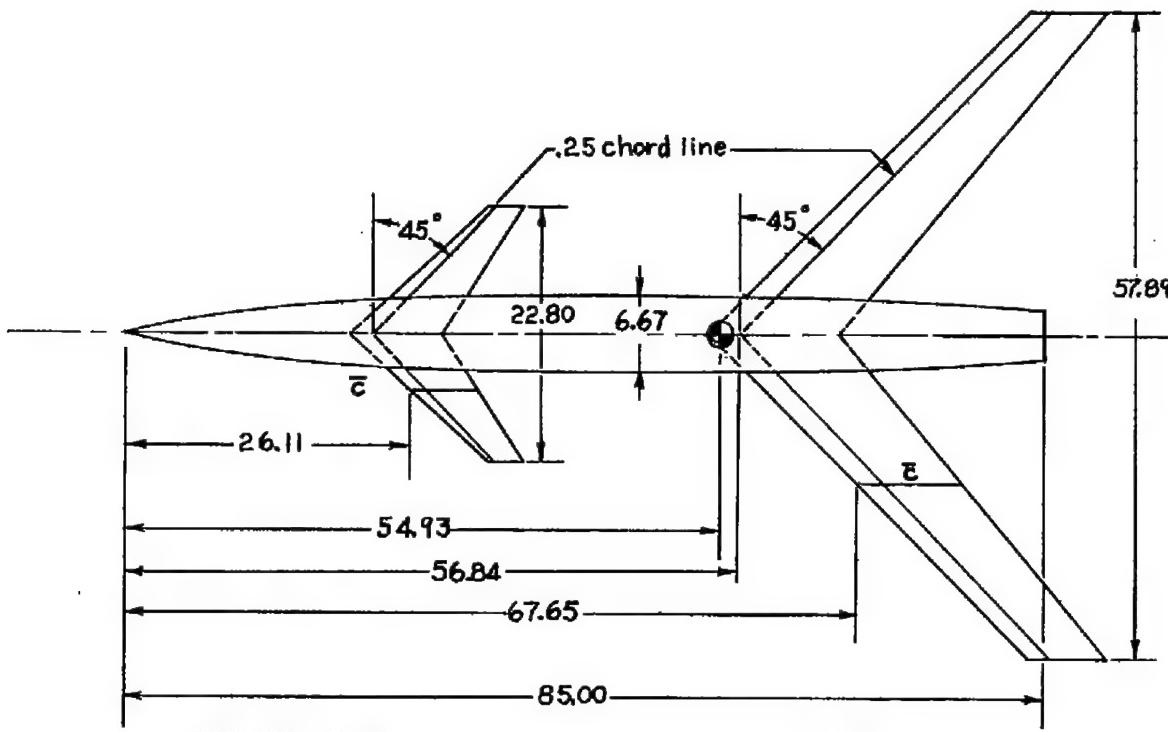
CANARD FINS
Airfoil   NACA 65A006

A	4.00
S (total)	.90 ft²
$\bar{c}$	6.05 in.
c (root)	8.15 in.
c (tip)	3.26 in.
Dihedral	0°
Incidence	0°

WING
Airfoil NACA 65A009

A	6.00
S (total)	3.88 ft²
$\bar{c}$	9.85 in.
c (root)	12.06 in.
c (tip)	7.24 in.
Dihedral	0°

(a) Canard configuration.

Figure 1.- Some physical characteristics of the canard configuration.
All dimensions in inches.
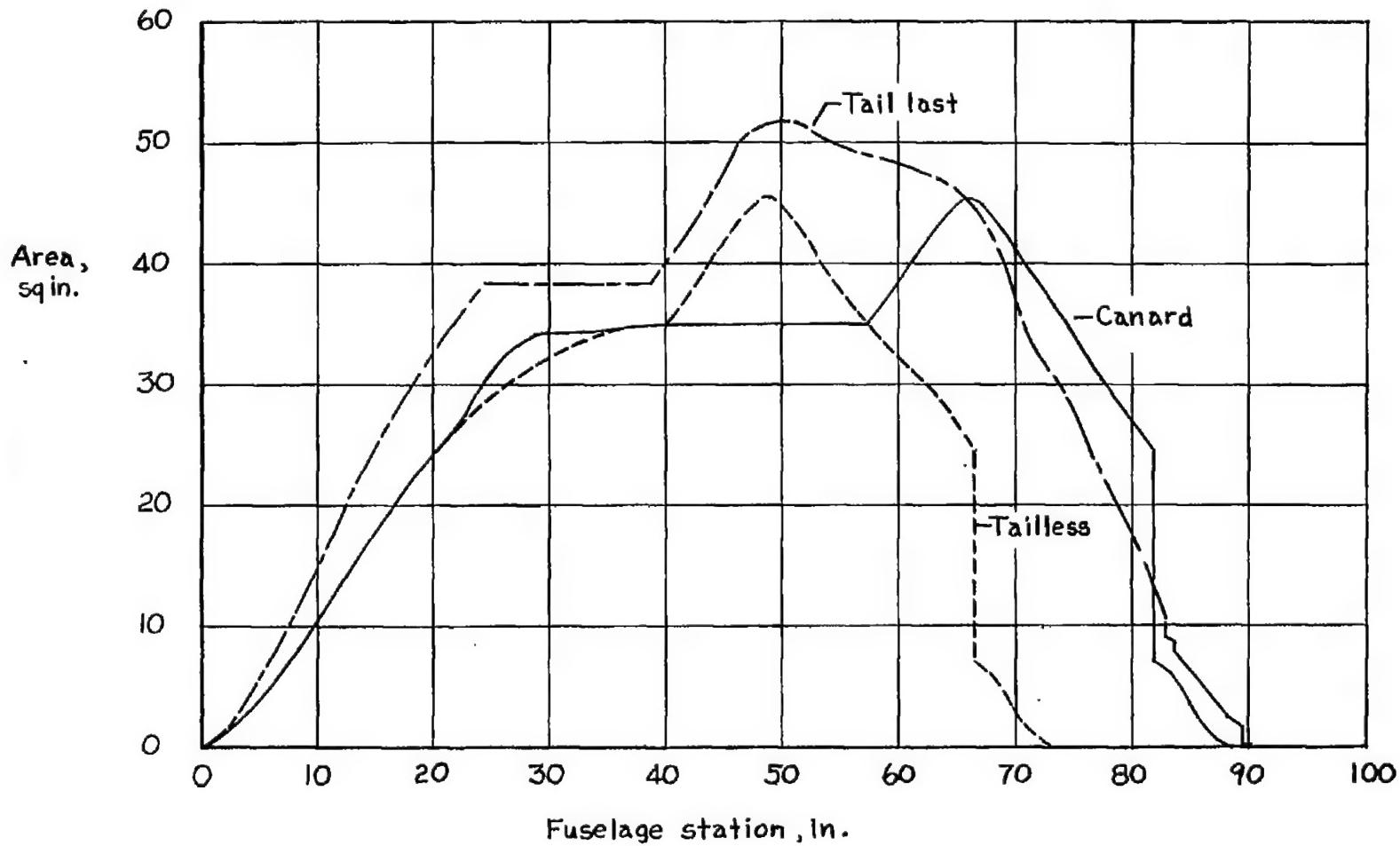
(b) Distribution of cross-sectional area along the body length.

Figure 1.- Concluded.

L-83998.1
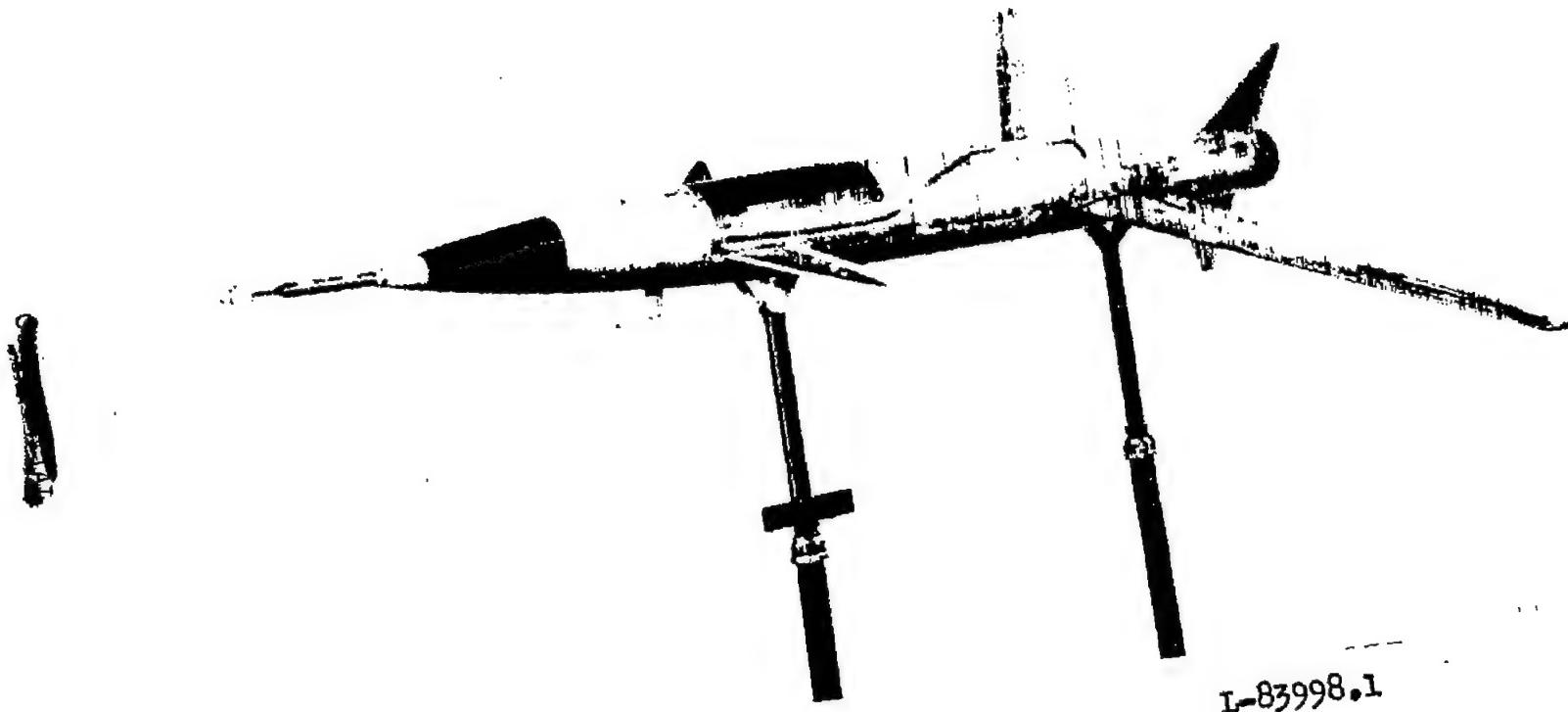
(a) Three-quarter front view.

Figure 2.- Photographs of the canard configuration.
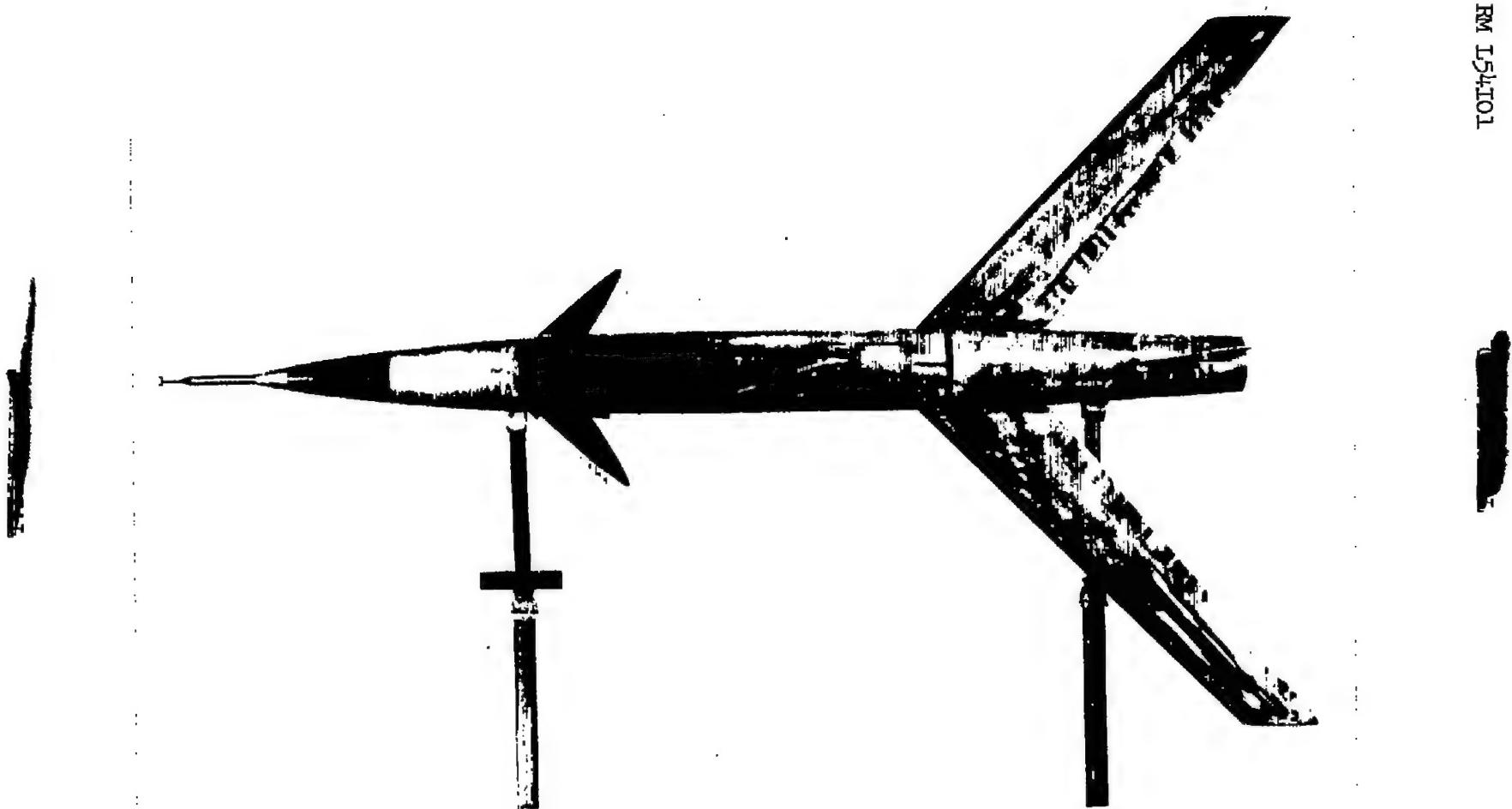
L-83997.1

(b) Top view.

Figure 2.- Concluded.
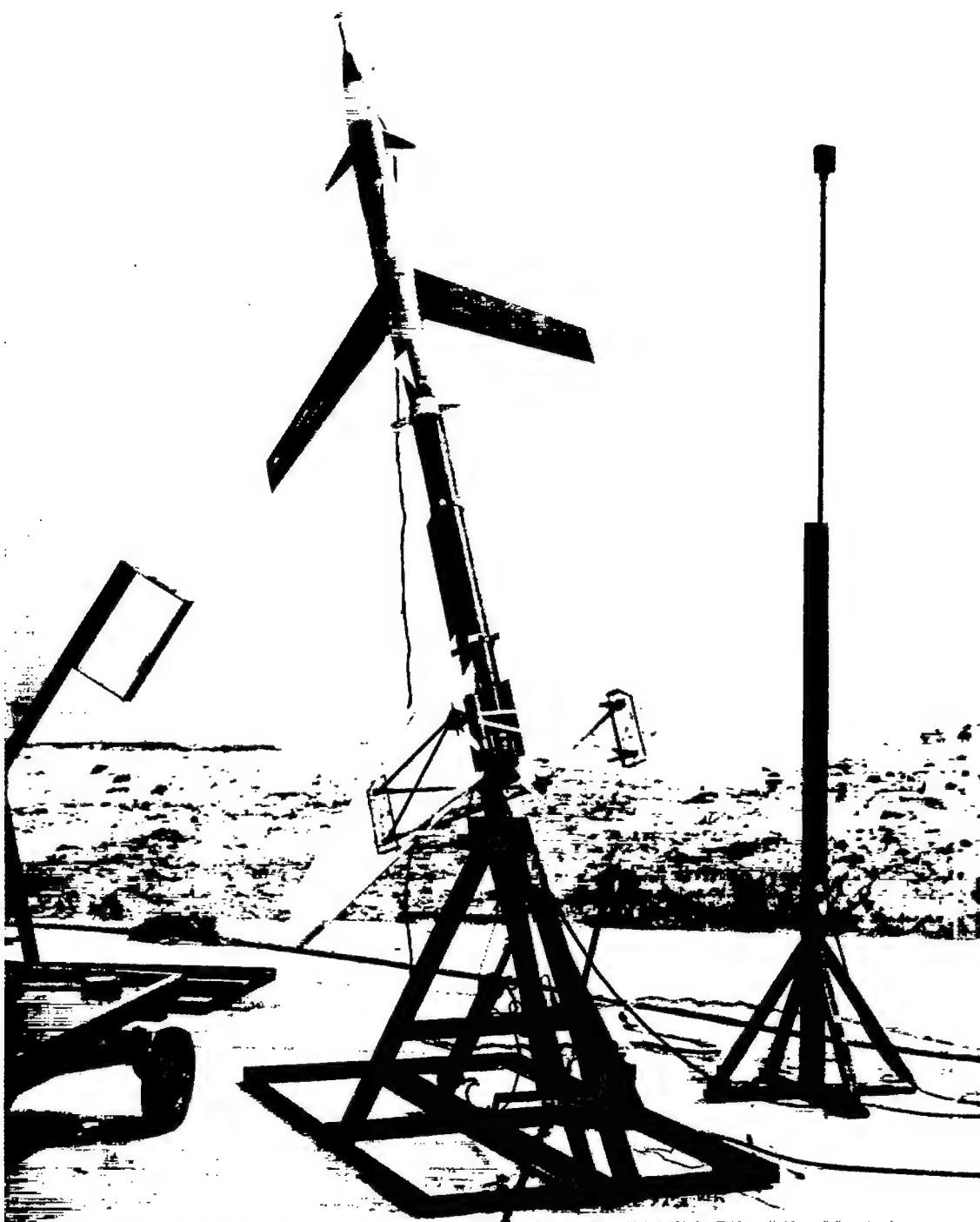
L-84397.1

Figure 3.- Model-booster combination on rail-type launcher.
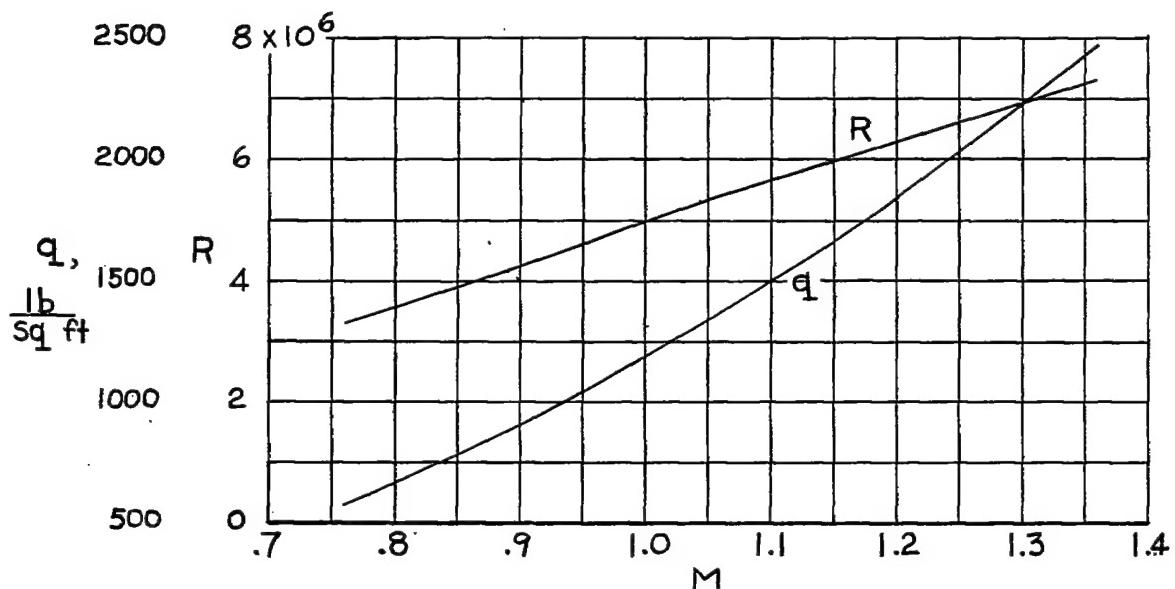
Figure 4.- Variation of Reynolds number (based on wing $\bar{c}$) and dynamic pressure with Mach number.
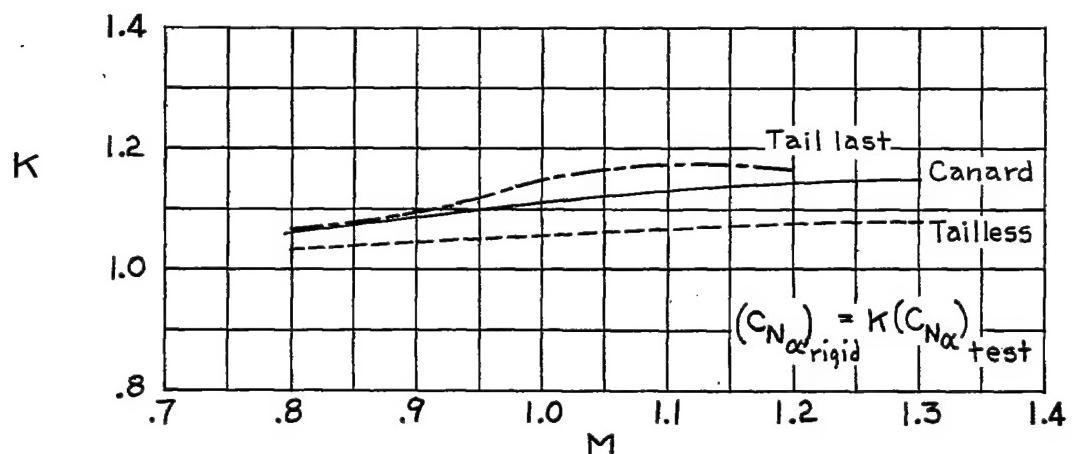
Figure 5.- Factor for obtaining values of rigid-wing lift-curve slope.
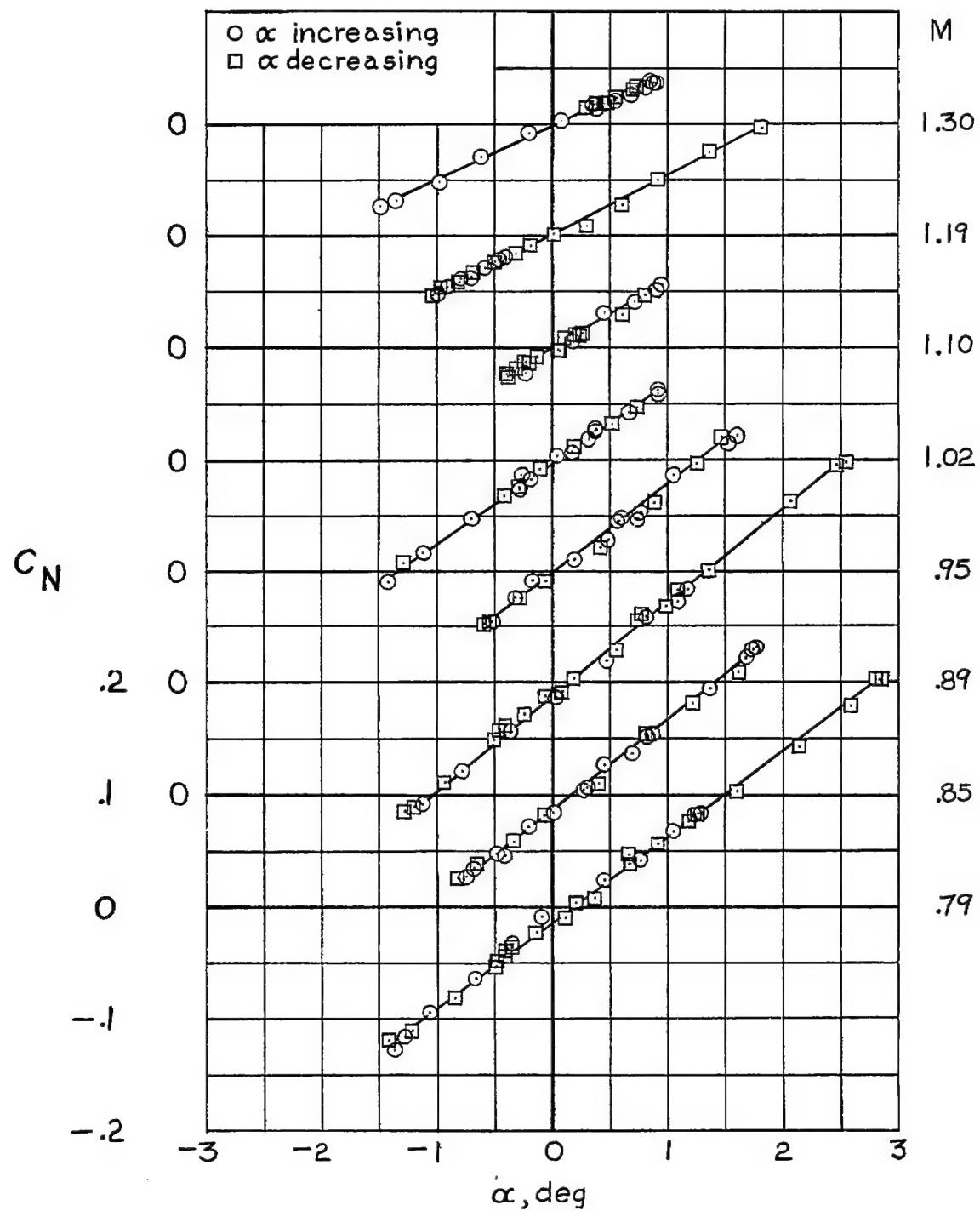
Figure 6.- Lift data for canard configuration.
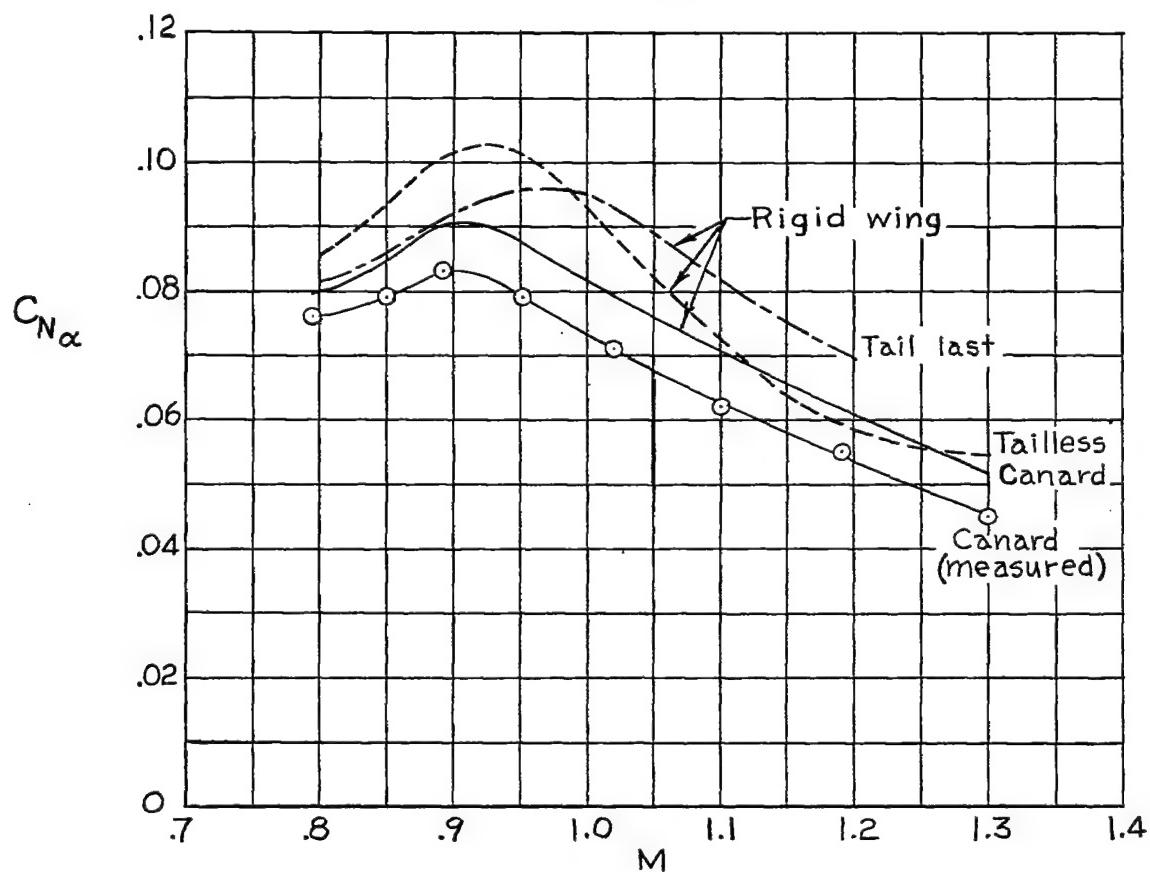
Figure 7.- Lift-curve slopes.
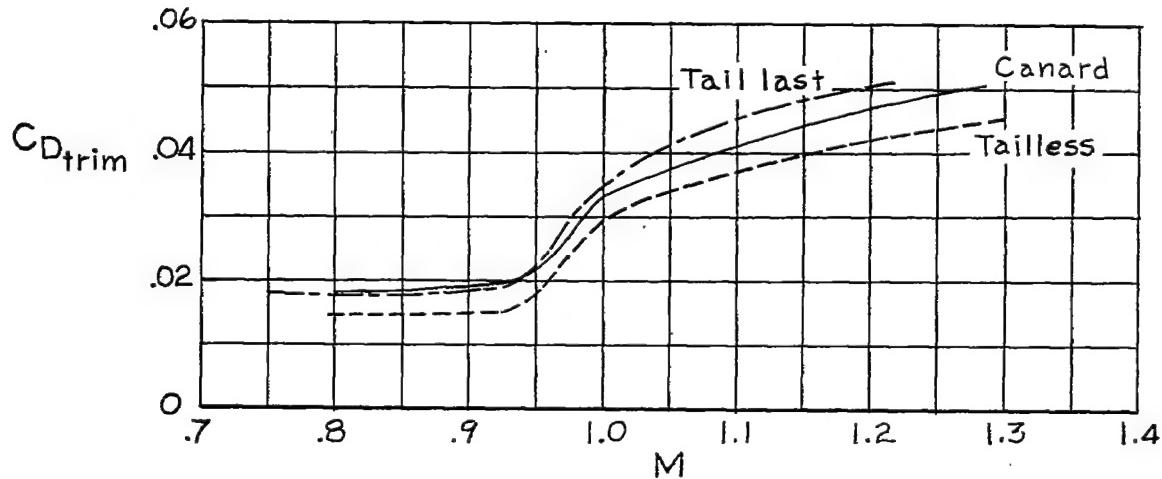
Figure 8.- Trim drag-coefficient variation with Mach number.
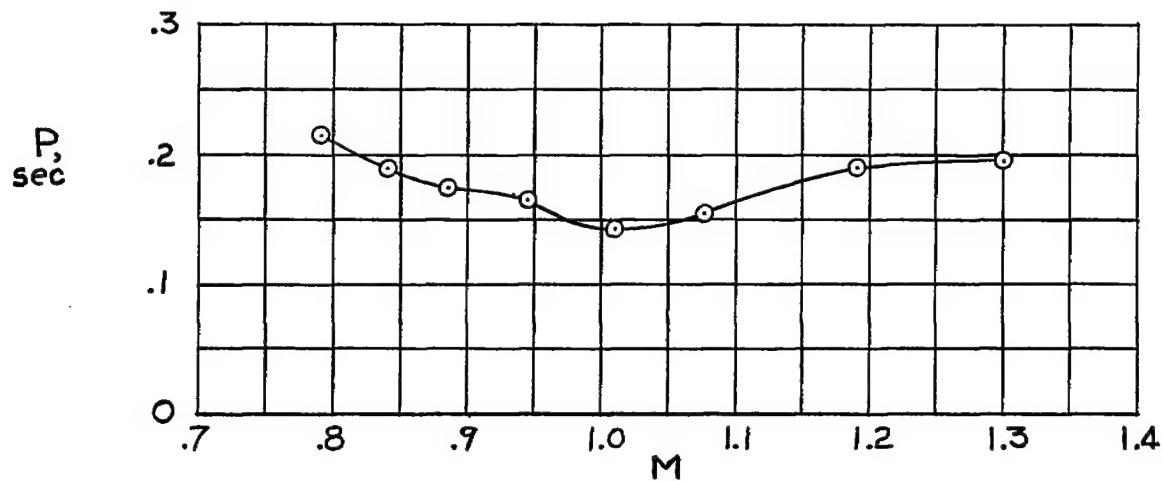
(a) Period of oscillation.
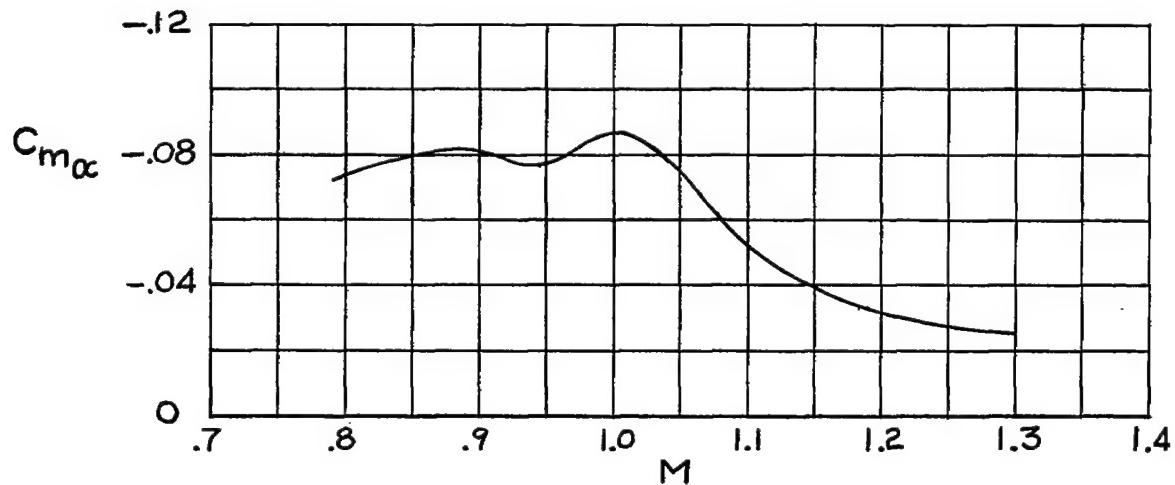
(b) Variation of pitching-moment-curve slope with Mach number.

Figure 9.- Static stability characteristics of the canard configuration.
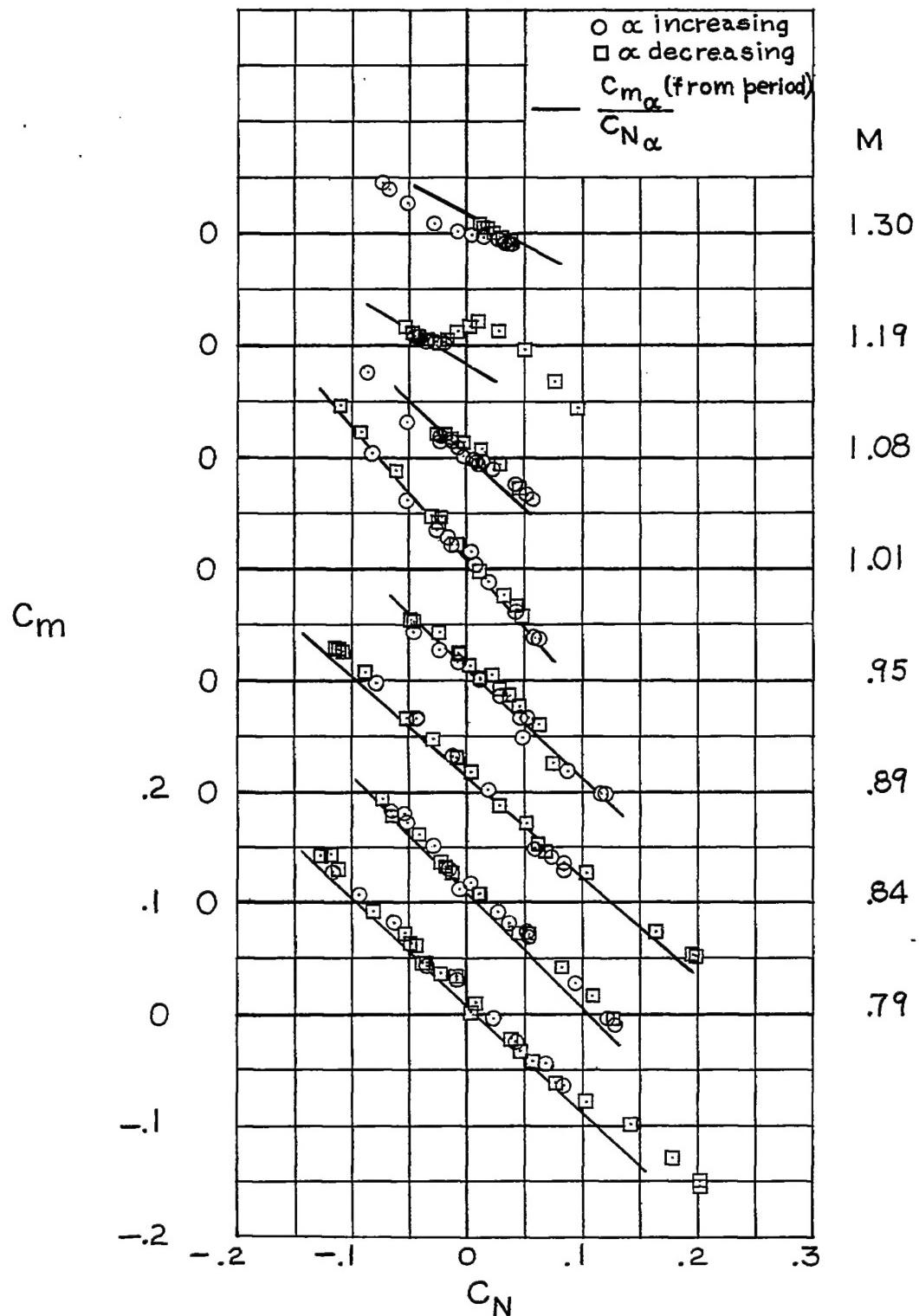
Figure 10.- Pitching-moment data for the canard configuration.
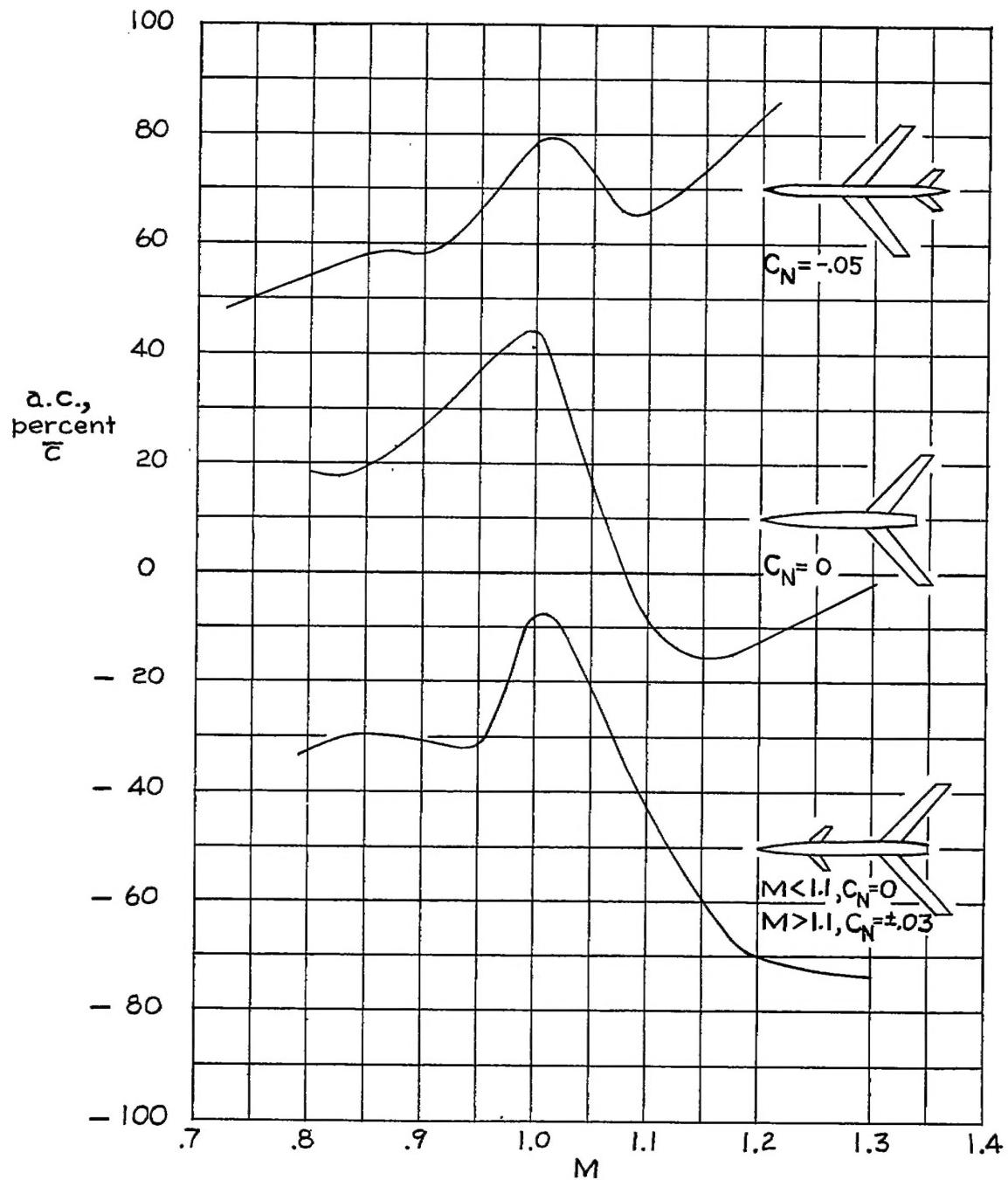
Figure 11.- Comparison of variation of aerodynamic-center movement for canard, tailless, and tail-last configurations.
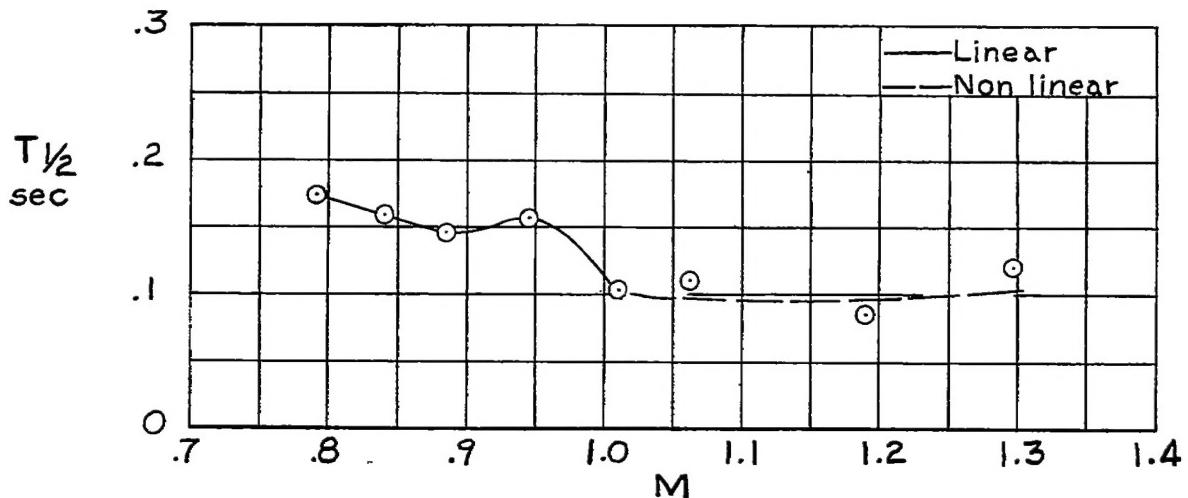
(a) Time for pitch oscillation to damp to one-half amplitude for canard configuration.
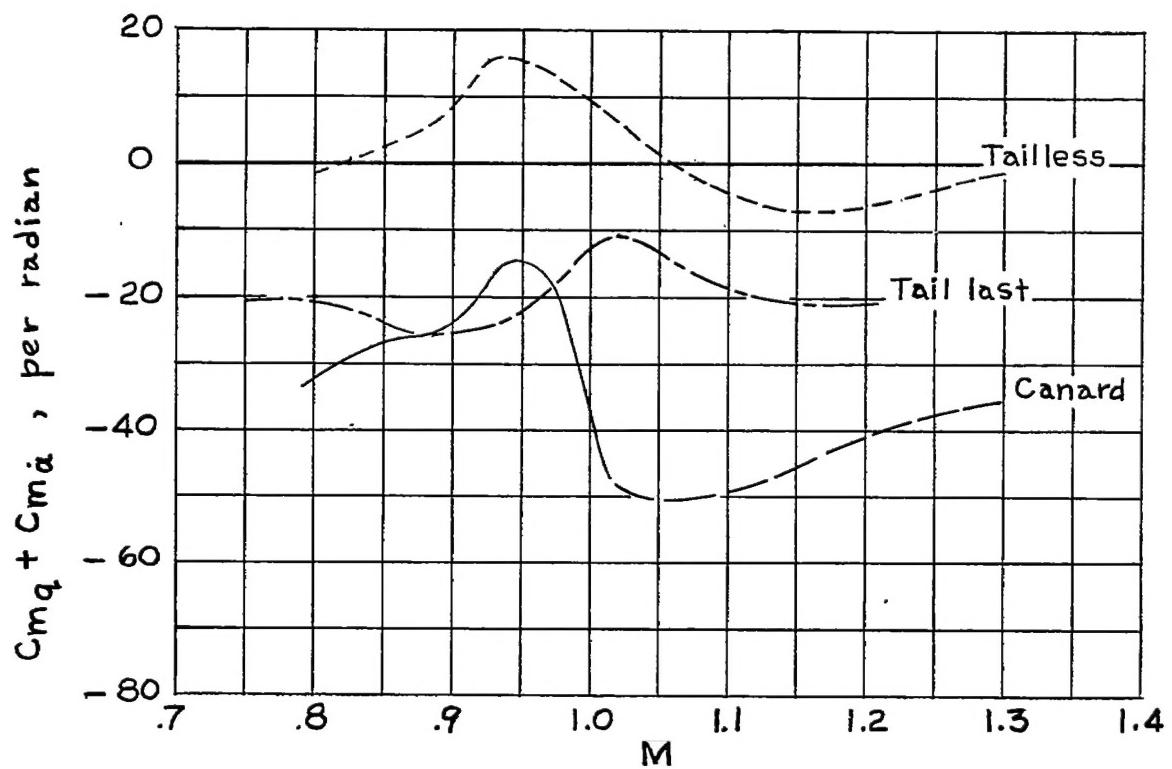

(b) Pitch-damping variation with Mach number.

Figure 12.- Dynamic-stability characteristics of canard, tailless, and tail-last configurations.
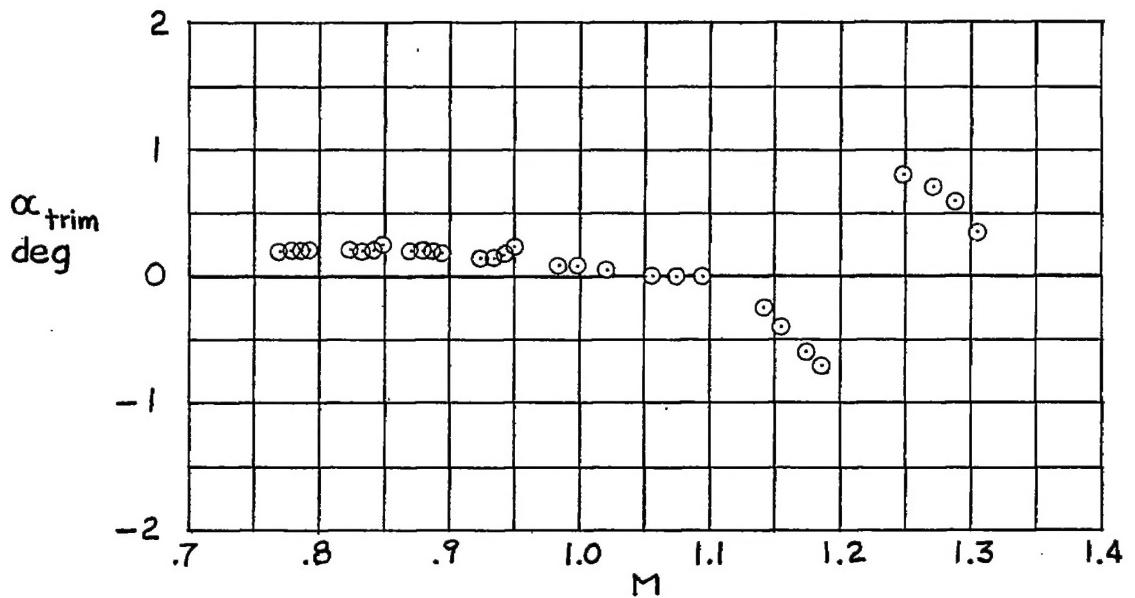
(a) Trim angle-of-attack variation with Mach number.
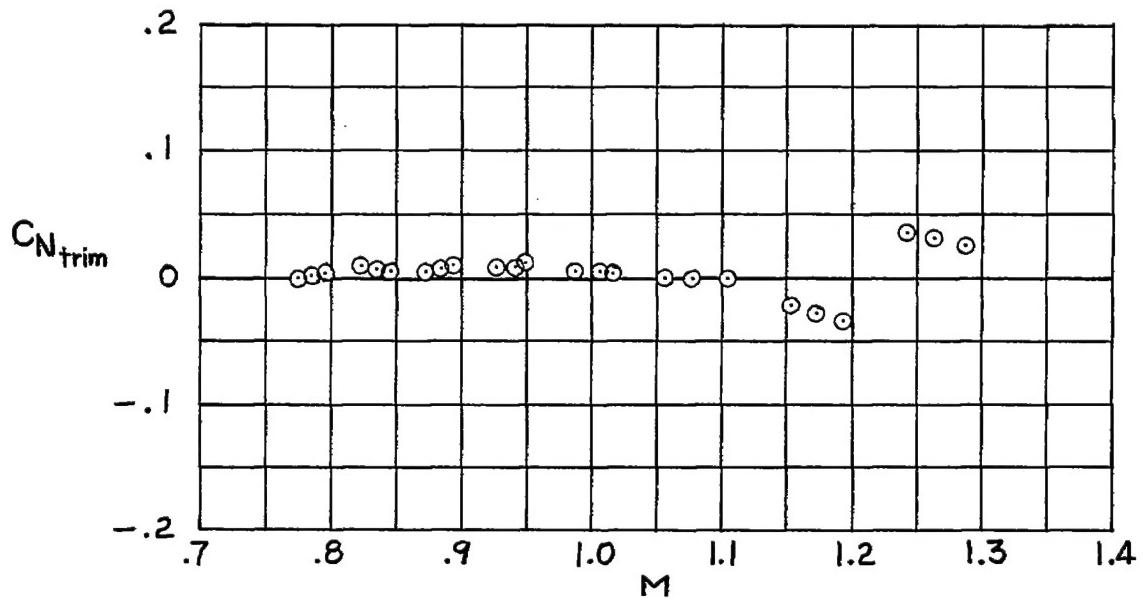
(b) Trim normal-force-coefficient variation with Mach number.

Figure 13.- Trim characteristics of the canard configuration.